

1 **CALIBRATION AND VALIDATION OF A WEATHER-RESPONSIVE  
2 ESTIMATION AND PREDICTION SYSTEM OF A MACROSCOPIC  
3 TRAFFIC FLOW MODEL**

4

5 Hanzel Mejia<sup>a</sup>, Ampol Karoonsoontawong<sup>b</sup>, Kunnawee Kanitpong<sup>c</sup>

6

7 <sup>a</sup>Department of Civil Engineering, Faculty of Engineering, Visayas State University,  
8 Visca, Baybay City, 6521, Leyte, Philippines.

9 <sup>b</sup> Department of Civil Engineering, Faculty of Engineering, King Mongkut's University  
10 of Technology Thonburi, Bangkok 10140, Thailand.

11 <sup>c</sup>Department of Civil Engineering and Infrastructure Engineering, School of  
12 Engineering and Technology, Asian Institute of Technology, Klong Luang,  
13 Pathumthani 12120, Thailand.

14

15 **Abstract:** This study evaluates the METANET model's capability to simulate traffic  
16 dynamics under normal and adverse weather conditions, confirming its reliability in  
17 forecasting real-world traffic behavior, particularly in regions with frequent rainfall.  
18 Calibration and validation results demonstrate METANET's adaptability, with critical  
19 parameters such as free-flow speed, capacity, and critical density significantly  
20 influencing performance. Adjusting these parameters enhances METANET's  
21 responsiveness to weather-induced traffic flow variations, providing a robust  
22 foundation for developing weather-responsive traffic management systems. The study  
23 successfully replicates METANET's predictive performance using traffic data from  
24 Bangkok, Thailand, marking the first application of the model in this region. Findings  
25 suggest that accounting for traffic flow heterogeneity only marginally improves  
26 accuracy, likely due to the limited study area and its relatively homogeneous traffic  
27 conditions. Validation results indicate that weather-specific modeling outperforms  
28 general models, effectively capturing congestion onset and dissipation while accurately  
29 predicting spatiotemporal traffic variations. Weather-adaptive METANET models  
30 demonstrate improved accuracy in tracking congestion waves and replicating flow-  
31 density relationships under varying rainfall intensities. The research underscores the  
32 model's sensitivity to key traffic parameters, emphasizing the necessity of  
33 incorporating weather considerations into traffic flow modeling for more precise  
34 predictions.

35

36 **1. INTRODUCTION**

37 Weather conditions impact various road conditions, including traffic demand, safety,  
38 operations, and flow. This paper proposes including rainfall factors in macroscopic  
39 traffic flow modeling, calibrated and validated using field data. This model aims to  
40 calculate the effects of rainfall on traffic flow dynamics, which has potential  
41 applications for traffic control and operations.

42 Macroscopic traffic flow theory is used to predict states of traffic at any segment of a  
43 highway based on initial conditions. The model treats the flow of traffic as a fluid rather  
44 than focusing on individual vehicles, using three main variables - average speed,

45 density, and flow - to describe traffic stream characteristics. Macroscopic traffic flow  
46 models are classified as first-order, second-order, or higher-order models, depending  
47 on the number of differentials. In literature, two widely used macroscopic models are  
48 used. The first is the CTM or the Cell Transmission Model, and the other is the  
49 METANET model. In a systematic review of well-known papers on macroscopic  
50 traffic flow modeling by Wang et. al (Wang et al., 2022), they looked into 32 papers,  
51 of which 80 % either used CTM or METANET.

52 The Lighthill–Whitham–Richards (LWR) model (Lighthill & Whitman, 1955;  
53 Richards, 1956) is a popular first-order model, employing a single PDE in expressing  
54 the flow following the law of conservation of vehicles. In a well-known paper by  
55 Daganzo (Daganzo, 1994), he introduced the Cell Transmission Model (CTM), which  
56 represents the road as a series of discrete cells, each of which can hold a certain number  
57 of vehicles. Vehicles move between cells according to specific rules, allowing the  
58 model to capture traffic flow, congestion, and other traffic dynamics in a simplified yet  
59 effective manner. It is a discretized version of LWR, which can be solved analytically  
60 due to its piecewise linear Fundamental Diagram (FD). While both can determine the  
61 uncongested and congested side of the FD representing normal traffic and congestion,  
62 they cannot replicate complex phenomena. Examples of this are the capacity drop  
63 phenomenon and scattering in the  $q-k$  (flow density) diagram.. Higher-order models  
64 have solved these limitations. Several approaches have been developed to enhance the  
65 LWR model and its ability to simulate complex traffic phenomena.

66 The Payne-Witham (PW) Model, introduced by Payne (Payne, 1971) and Whitman  
67 (Whitman, 1974), derives the equation for acceleration using the expanded Taylor  
68 series of a car-following model. It offers insights into complex traffic phenomena such  
69 as scattering in the flow-density diagram. A discretized version of this model,  
70 METANET, was proposed by Messmer and Papageorgiou (Messmer & Papageorgiou,  
71 1990) and is widely used for large-scale network applications and control purposes  
72 (Kontorinaki et al., 2017; Kotsialos et al., 2002; Papageorgiou et al., 2010; Spiliopoulou  
73 et al., 2014, 2017). The METANET model is a macroscopic discrete second-order  
74 model that was firstly applied to the Boulevard Périphérique in Paris. The name  
75 METANET, acronym for "Modèle d'Écoulement de Trafic sur Autoroute NETworks"  
76 in French which translates to "Traffic Flow Model on Highway Networks", was firstly  
77 associated with the simulation tool for the freeway network, but it is now adopted to  
78 generically indicate the second-order traffic flow model.

79 In the study of Spiliopoulou et al. (2014), which compared traffic flow modeling using  
80 the Cell Transmission Model and METANET, they showed that the second-order  
81 model METANET performed better than CTM. Kontorinaki et al. (2017) also conclude  
82 that METANET outperforms other macroscopic models such as CTM and LWR and  
83 their extensions. In a comprehensive benchmarking of macroscopic traffic flow models  
84 conducted by Mohammadian et al. (Mohammadian et al., 2021), they compared the  
85 performance of the following models: LWR, LWR with extensions, CTM, CTM with  
86 extensions, METANET, Gas-Kinetic Theory, and Generic Second-Order Modeling.  
87 The models were assessed for their effectiveness in tracking congestion. Their findings  
88 indicated that METANET demonstrated the best performance overall, particularly  
89 excelling in modeling ramp-merging congestion.

90 This paper focuses on the METANET model, a discretized and improved variation of  
91 the LWR model combining the characteristics of the PW model. METANET is chosen  
92 for its three distinct dynamic functions that predict key traffic flow parameters: flow,  
93 speed, and density. Its form and convenient discretization intervals allow to facilitate  
94 the integration of field-collected data. The METANET model's clear analytical  
95 properties, including a specific space-time form with improved differentiable functions,  
96 make it suitable for real-time freeway traffic control operations. METANET has been  
97 applied across a range of areas, including Freeway Traffic Flow Modeling, where it has  
98 been utilized to model freeway traffic dynamics (Kontorinaki et al., 2017;  
99 Mohammadian et al., 2021; Spiliopoulou et al., 2017; Wang et al., 2022), variable speed  
100 limit control which was applied to manage and control variable speed limits (Wang et  
101 al., 2021), ramp metering where the model has been used to optimize strategies for  
102 metering of ramps (Kan et al., 2016; Wang et al., 2014, 2021), and traffic state  
103 estimation and prediction which has been employed for estimating and predicting traffic  
104 states (Wang et al., 2022; Zhao, 2021).

105 The weather-specific METANET model is calibrated and integrated into a validation  
106 model using field data. This paper makes four main contributions: First, it considers  
107 different weather conditions for calibration and applies them to various macroscopic  
108 traffic variables during validation, whereas, to our knowledge, previous studies have  
109 typically focused only on the applicability of weather-specific parameters and not on  
110 comparing them with other weather conditions. Second, it utilizes real field data rather  
111 than simulation data to provide clear quantitative results, demonstrating the significant  
112 impact of weather on freeway traffic dynamics. Lastly, it demonstrates the effects of  
113 considering multiple fundamental diagrams for every section of the highway.

## 114 2. METHODOLOGY

115 This paper focuses on the METANET model, a widely used macroscopic traffic flow  
116 model shown to outperform other models like the Cell Transmission Model (CTM) in  
117 accurately tracking freeway congestion. METANET is based on a discretized, enhanced  
118 version of the Payne-Witham model. It predicts key traffic parameters (flow, speed, and  
119 density) through three dynamic functions, making it suitable for real-time freeway  
120 traffic control. This paper aims to calibrate and validate METANET using a section of  
121 Bangkok's Burapha Whiti Expressway, which includes ramps and is subject to  
122 recurring congestion.

123 METANET divides the highway into sections and computes traffic states at each  
124 discrete time step. It uses equations involving density, flow, and speed, enhanced by  
125 additional terms for accurate on-ramp merging and lane-drop modeling. Calibration  
126 aligns model predictions with actual traffic data, while validation tests model  
127 performance on an independent dataset, focusing on average speed and flow as  
128 performance metrics. This process is optimized using the Nelder-Mead algorithm,  
129 selected for its efficiency in achieving accurate parameter estimates.

130 Traffic data, including flow, speed, and density, were collected every five minutes  
131 throughout 2022, covering both dry and rainy conditions. Two days of data were used  
132 for calibration (one with rain, one without), and six additional days were used for  
133 validation, ensuring no incidents or sensor failures during the study period.

137

138 METANET employs the discretization and enhancement of the form of the **Payne**  
 139 model. It treats the highway section as continuous numbered sections  $i$  (section  $i$  is  
 140 downstream of section  $i-1$ ), each with specific lengths  $L_i$ , and lane numbers  $\lambda_i$ . Time  
 141 is subdivided into equal gaps of duration  $T$ . In every discrete time step, time  $k = 0, 1, \dots,$   
 142  $K$ , METANET computes the density, flow, and speed for each section  $i$  using the  
 143 equations:

144

$$145 \quad \rho_i(k+1) = \rho_i(k) + \frac{T}{L_i \lambda_i} [q_{i-1}(k) - q_i(k)] \quad (1)$$

$$146 \quad q_i(k) = v_i(k) \rho_i(k) \lambda_i \quad (2)$$

$$147 \quad v_{i+1}(k) = v_i(k) + \frac{T}{L_i} v_i(k) [v_{i-1}(k) - v_i(k)] + \frac{T}{\tau} [V^e(\rho_i(k)) - v_i(k)] - \frac{v T [\rho_{i+1}(k) - \rho_i(k)]}{\tau L_i [\rho_i(k) + \kappa]} \quad (3)$$

148

149 Where the model parameters are a time constant ( $\tau$ ), an anticipation constant ( $v$ ), and a  
 150 mode parameter ( $\kappa$ ).  $V^e(\rho_i(k))$  represents the fundamental diagram and is determined  
 151 using the following equation:

$$152 \quad V^e(\rho_i(k)) = v_{f,i} \exp \left[ -\frac{1}{a_i} \left( \frac{\rho_i(k)}{\rho_{cr,i}} \right)^{a_i} \right] \quad (4)$$

153 where  $v_{f,i}$  represents the free-flow speed,  $\rho_{cr,i}$  represents the critical density  
 154 corresponding to the maximum flow condition, and  $a_i$  another model parameter. It  
 155 must be noted that the average speed calculated must be at least  $v_{min}$ .

156 For more accurate merging and lane-drop modeling, enhancements were proposed by  
 157 Papageorgiou et al. (1989). Specifically, the model incorporates two additional terms  
 158 to capture these effects better. One notable term addresses the on-ramp merging impact  
 159 by adjusting the traffic flow dynamics for the influence of merging cars. The following  
 160 term is then added

$$161 \quad -\delta T q_\mu(k) v_i(k) / L_i \lambda_i (\rho_i(k) + \kappa)$$

162 into eq. (3) for the on-ramp segment. A further parameter  $\delta$  is included, and  $q_\mu$   
 163 represents the number of vehicles entering the ramp. To include the consideration of  
 164 the effects of lane-changing, the term

$$165 \quad -\varphi T \Delta \lambda \rho_i(k) v_i(k)^2 / L_i \lambda_i \rho_{cr,i}(k)$$

166 is included to eq. (3) for the consideration of the immediate section upstream when  
 167 there is a dropping of lanes, a model parameter  $\varphi$  is further added where  $\Delta \lambda$  refers to  
 168 the number of lanes that were dropped.

169 At the change of geometric characteristics, such as the presence of ramps, the flow is  
170 separated into various sections that exit on the highway based on a defined turning rate  
171  $\beta_j(k)$ . Additionally, for sections entering the change in highway geometry, a density  
172 downstream  $\rho_i(k+1)$  is required in eq. (3) to account for the influence of downstream  
173 traffic conditions. Given that bifurcations lead to two downstream sections, the  
174 following is used to determine the downstream density for section  $i$  at the bifurcation  
175 as proposed by Messmer & Papageorgiou (1990):

176 
$$\rho_{i+1}(k) = \frac{\sum_{\mu \in O_i} \rho_{\mu}^2(k)}{\sum_{\mu \in O_i} \rho_{\mu}(k)} \quad (5)$$

177 where  $\rho_{i+1}(k)$  represents the computed downstream density under consideration utilized  
178 in eq. (3) for section  $i$ . Meanwhile,  $\rho_{\mu}(k)$  denotes the section density downstream of  
179 considered segment, where  $O_i$  is the set of sections which exits the highway. The  
180 quadratic average used in eq. (5) considers the potential congestion spillback to the  
181 section. The eq. (5) does not require any additional calibration parameters. For this  
182 study, the actual densities on off-ramps are given as boundary conditions to the model.  
183 Consequently, any increase in the density of the off-ramp directly affects the average  
184 speed of the upstream mainstream area through equations eq. (3) and eq. (5). For  
185 merging locations with on-ramps, the model incorporates the actual on-ramp flows as  
186 direct input, treating on-ramps as integrated parts of the sections rather than modeling  
187 them as separate entities.

188 METANET modeling includes various parameters whose values can vary depending  
189 on factors like the network geometry, driver behavior, truck percentage, and weather  
190 conditions at different freeway sites. Therefore, the accuracy and reliability of these  
191 models depend on correctly specifying these parameter values. Calibration of the  
192 models is often necessary to ensure they are suitable for real-world applications while  
193 validation tests the accuracy of the model.

194

## 195 **2.1 Calibration and validation of models**

196

197 Before applying traffic models to practical applications like traffic monitoring and  
198 management, they must undergo calibration and validation using actual traffic data.  
199 Calibration adjusts model parameters to minimize the difference between predictions  
200 and observed data, ensuring the model accurately reflects current traffic conditions.  
201 Validation tests the calibrated model's predictive performance using an independent  
202 dataset, assessing its ability to predict future traffic. Both processes are critical:  
203 calibration without validation has limited value, as it only fits the model to a specific  
204 dataset without ensuring broader applicability.

205

206 Calibration also estimates parameters not directly observable in the dataset, especially  
207 in higher-order models like METANET, which include empirical terms to enhance  
208 modeling capabilities. This process typically involves solving nonlinear systems  
209 through optimization techniques to minimize the difference between model outputs and  
210 actual data using a cost function. Parameter values are selected from an admissible  
211 range defined by prior experience and physical meaning.

212

213 Validation uses a different dataset (e.g., from another day) within the same study area  
214 to compare model outputs with actual data, ensuring the model performs reliably across

215 various traffic conditions and time periods. While flows are easier to model due to  
216 conservation equations, accurately predicting average speeds across highway segments  
217 remains challenging.

218  
219 Calibrating a least-squares optimization problem nonlinearly often has multiple local  
220 minima as illustrated by Ngoduy & Maher (2012) in the calibration of second-order  
221 traffic models using the continuous cross-entropy method, making gradient-based  
222 methods unsuitable. Spiliopoulou et al. (2017) demonstrated that different optimization  
223 techniques can arrive at solutions to the estimation problem for METANET. They have  
224 employed three commonly used optimization algorithms. The first is the Nelder-Mead  
225 (N-M) algorithm (Lagarias et al., 1998; Nelder & Mead, 1965) which is deterministic.  
226 The next one is the stochastic Genetic Algorithm (GA) (Whitley, 1994). Lastly, they  
227 also considered the cross-entropy method (Rubinstein & Kroese, 2004). All three  
228 algorithms were able to converge to a solution set. Nevertheless, their results show that  
229 the Nelder-Mead algorithm performs 257 times faster than the genetic algorithm and  
230 242 times faster than the cross-entropy method. This is an important finding since the  
231 computation time must be considered in traffic flow modeling, especially because it  
232 often involves real-time applications. Therefore, the Nelder-Mead Algorithm is used in  
233 this study for the determination of the parameters. The algorithm is also well-suited for  
234 finding acceptable local minima, or potentially even the global minima, in complex,  
235 multi-dimensional optimization landscapes.

236

## 237 **2.2 The Nelder-Mead algorithm**

238

239 The Nelder-Mead algorithm (Nelder & Mead, 1965) is a renowned algorithm for the  
240 optimization of multidimensional systems with unconstrained conditions. For this  
241 study, we have particularly adapted a version for constrained optimization as described  
242 by Spiliopoulou et al. (2014). This method is advantageous because it requires no  
243 derivative information, making it applicable for problems with nonlinear and  
244 discontinuous cost functions.

245

246 The algorithm operates using a simplex with  $n$  number of dimensions and  $n+1$  number  
247 of vertices. Each vertex represents a potential solution and has an associated cost  
248 function value. The Nelder-Mead method begins with an initial simplex and iteratively  
249 transforms it to increase the predictive accuracy at the vertices. In every iteration, the  
250 method will sort the solutions by their cost function values, calculate the centroid, and  
251 then update the solution by reflecting, expanding, or contracting the worst vertex. If  
252 these transformations do not yield improvements, the algorithm performs a shrinkage  
253 towards the best vertex, generating new vertices.

254

255 The algorithm's performance is influenced by the four parameters of  $\sigma$  for shrinkage,  $\chi$   
256 for expansion,  $\xi$  for reflection, and  $Y$  for contraction. The recommended values for  
257 these parameters are 0.5, 2, 1, and 0.5, respectively (Spiliopoulou et al., 2014). The  
258 algorithm may sometimes perform many iterations without significant improvements.  
259 To address this, multiple restarts with a limited number of iterations can be used as a  
260 heuristic solution. This technique was employed in this paper by doing 5 runs for each  
261 calibration and comparing the respective performances.

262

263

264

265 **2.3 Measurement of performance**

266  
267 In this context, measuring performance involves assessing key variables used to  
268 evaluate the results of model calibration. For macroscopic traffic flow modeling, the  
269 primary variables are flow in veh/hr, density in veh/km, and average speed in km/hr.  
270 The calibration process is compared against the actual dataset, which is also represented  
271 by these traffic flow variables. Therefore, evaluating calibration results based on these  
272 variables is natural. From the modeling results of other papers, it is advisable to focus  
273 on average speeds during the calibration procedure. This is because empirical  
274 observations suggest predicting flows is relatively straightforward due to the  
275 conservation law, even if speed matching is not perfect.

276  
277 Second, it has been found that if the modeled speeds match the actual speeds in the  
278 segment considered adequately, the flow predictions are generally satisfactory. Thus,  
279 focusing on speed matching is crucial and often more challenging. Lastly, measuring  
280 densities directly or modeling occupancies is difficult, with data often being incomplete  
281 or inaccurate.

282 **2.4 Test Network, Evaluation, and Traffic Data**

283  
284 A highway network is graphically represented where links correspond to segments of  
285 the highway with consistent characteristics, such as uniform lane count, grade, and  
286 curvature. Nodes are used to indicate significant changes in the roadway's geometry  
287 including ramps and lane reductions. If a segment exhibits varying characteristics, it is  
288 divided into multiple links, each separated by a node.

289  
290 For computational modeling, the time horizon is divided into 5-second intervals. To  
291 ensure the stability of the numerical method, the length of each segment and the time  
292 interval must satisfy the celebrated Courant-Friedrichs-Lowy (CFL) condition (Courant  
293 et al., 1928; de Moura & Kubrusly, 2013; Sanz-Serna & Spijker, 1986).

294  
295 The study area considered for this paper is a segment of the Burapha Whiti Expressway  
296 in Bangkok, Thailand (station 12+400 to 19+500). This highway stretch includes on-  
297 ramps and off-ramps. This part of the expressway was considered for the calibration  
298 and validation of the traffic flow model because of the presence of the ramps. This is  
299 also the segment of the highway nearest to the automatic weather station. Only this span  
300 of the highway was considered to make the effects of weather more pronounced as  
301 different parts of the highway far from the weather station may experience a different  
302 effect on the traffic flow in consideration of weather. To model the study area by use  
303 of the METANET model, the highway is represented with four nodes and three links.  
304 Each node represents an area with a change in geometric characteristics in the highway.  
305 The homogenous highway segments in between are denoted by links. Figure 1 displays  
306 the length, number of lanes, ramp locations, and the location of the microwave radar  
307 detectors represented by bullets.

308  
309 The dataset for this study was gathered at the Expressway Authority of Thailand, which  
310 operates country's expressway system. It includes flow, speed, and density for each  
311 microwave radar station gathered every 5 minutes. It is observed that recurring  
312 congestion is evident in this area in the morning rush hours due to the presence of  
313 ramps. 2 days were selected for the calibration process, representing each for good and

315 bad weather conditions representing the occurrence of rainfall during the gathering of  
 316 data while 6 days were considered for validation (3 for each weather condition). It is  
 317 important to note that the primary criterion for selecting these 8 days was that no  
 318 incidents or detector failures occurred during the morning hours of 5–12 AM on the  
 319 examined freeway stretch, conditions which could not be replicated by any traffic flow  
 320 model. Figure 2.1 illustrates the detailed layout of this expressway and the locations of  
 321 traffic sensors, represented by black dots. Data for analysis were collected in 2022,  
 322 including days with and without precipitation.

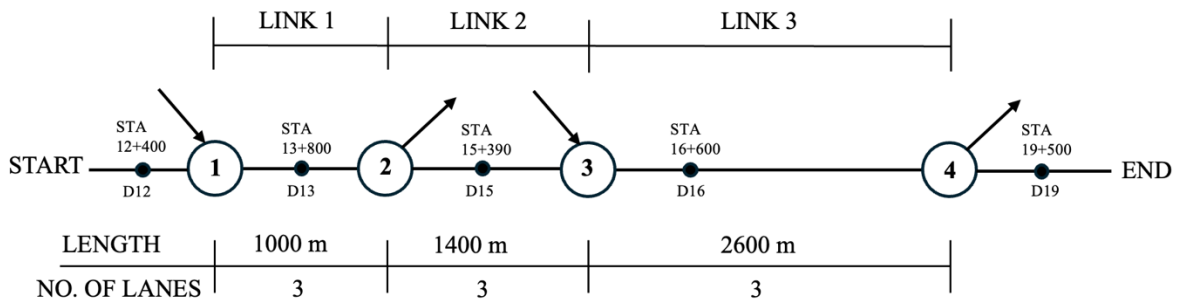
323

324

325 **Figure 1**

326

327 *Representation of the Study Area Considered in Burapha Whiti Expressway, Bangkok,*  
 328 *Thailand.*



329

330 **2.5 Novel Considerations**

331 This paper offers a comprehensive examination of macroscopic traffic flow modeling,  
 332 focusing on both calibration and validation. Unlike previous studies, this research  
 333 provides a more detailed analysis of model calibration, addressing critical aspects such  
 334 as congestion tracking, capacity reduction, and the impact of weather conditions on  
 335 prediction accuracy. It also includes extensive validation results from the same case  
 336 studies, demonstrating that the METANET model accurately captures traffic flow  
 337 dynamics, particularly concerning weather-specific conditions.

338 Despite the significance of calibrating models with real traffic data for accurate  
 339 application, there is a scarcity of research dedicated to model calibration and validation  
 340 (Wang et al., 2022). Furthermore, the numerical computation of these models  
 341 necessitates space-time discretization, making simplified and analytically tractable  
 342 models highly beneficial for practical applications.

343 This paper aims to address four key issues in traffic flow modeling:

344 a. Traffic Flow Inhomogeneity: stretches of a highway usually exhibit inhomogeneity  
 345 in traffic flow due to variations in key traffic flow parameters caused by several  
 346 factors. To effectively model such variations, a model must consider different  
 347 fundamental diagrams to represent a section of the highway with the same traffic  
 348 and geometric characteristics.

349 b. Congestion Tracking: this refers to a model's ability to reproduce and predict when  
350 recurrent congestions emerge and propagate. A model should accurately reproduce  
351 the dynamics of congested traffic flow across spatial and temporal scales. The  
352 effectiveness of a model in reflecting real-world traffic is determined by how its  
353 structure is represented mathematically and by the parameters the model includes.  
354 When it is established, the focus shifts to calibrating parameters to ensure the model  
355 can accurately describe the entire evolution of traffic conditions.

356 c. Effects of Weather on Macroscopic Traffic Flow Modeling: the performance of  
357 models that undergo calibrations under an unspecified weather event may not  
358 accurately represent the dynamics of traffic under different weather conditions in  
359 the same location, as key traffic parameters can be significantly affected. In the  
360 literature, only the work of Bie et al. (2017) specifically addressed and investigated  
361 the impact of weather parameters on traffic dynamics using METANET by  
362 introducing a weather factor into macro traffic state prediction. There is limited  
363 quantitative evidence on the broader impact of weather on model performance. This  
364 research will also address model parameter transferability, evaluating whether a  
365 calibrated model remains applicable to new datasets from different times or weather  
366 conditions, a topic that has not been fully explored in the literature. The focus will  
367 be on determining if a model developed with normal weather data can be effectively  
368 used for rainy or other adverse weather conditions, and vice versa.

369 This research seeks to provide empirical evidence and enhance the understanding  
370 of these issues, which are currently supported more by qualitative observations than  
371 by quantitative analysis.

### 372 **3. RESULTS AND DISCUSSION**

#### 373 3.1 Model Calibration Result under Normal Weather Conditions

374 The different results of the calibrations are detailed in this section, focusing first under  
375 normal conditions. The data for June 9, 2022, was used for this. For not accounting for  
376 traffic flow heterogeneity, the specific results are illustrated in Figures 3.1 and 3.2.  
377 When considering for heterogeneity, the summary of the performance with specific  
378 results illustrated in Figures 3.3 through 3.4.

379 The Nelder–Mead algorithm was employed for calibration with the following settings:  
380  $\xi = 1$ ,  $\chi = 2$ ,  $\gamma = 0.5$ , and  $\sigma = 0.5$  (for further details, see Section 2.2). The algorithm  
381 was terminated based on either the convergence of the cost function or the convergence  
382 of the acceptable simplex, both when the tolerance level reaches 0.1, and after 500  
383 iterations.

##### 384 3.1.1 Not Considering Heterogeneity

385 As discussed in the previous sections, not accounting for traffic flow inhomogeneity  
386 means that only 1 fundamental diagram (FD) is considered for the whole study area.  
387 Analysis of the measurement data revealed that the highway under consideration has  
388 the same geometric characteristics.

389 Five calibration runs were conducted, and their performance is measured in terms of  
390 Mean Absolute Percentage Error (MAPE) for all the detectors. For each calibration run,  
391 the algorithm begins with specified initial values and randomly generates the next

values based on these initial values. As described in the previous sections, the working simplex consists of  $n + 1$  vertices, where  $n$  represents the number of parameters being calibrated. Using a physically reasonable initial vertex is preferable to expedite algorithm convergence. The results show that the best performance of all the calibration runs has a MAPE of 1.3943 %, 3.1043 %, and 5.7205 % for Detectors 13, 15, and 16, respectively. Nevertheless, the difference in the performance index between each run is not very significant, showing that the algorithm converges to almost the same optimal parameters. The best run will be used for further analysis.

Table 3.1 presents the optimum parameter values calculated by the Nelder-Mead algorithm for the best calibration run.  $\tau$  is the relaxation time parameter in second (s) which impacts how fast the average speed can cope with the speed in equilibrium that is computed in the FD,  $\nu$  is an anticipation parameter in  $\text{km}^2/\text{h}$  controlling the backward movement of the congestion wave,  $\delta$  is a parameter controlling the merging mechanism in  $\text{h}/\text{km}$ ,  $\Phi$  is the parameter responsible for the dropping of lanes in  $\text{h}/\text{km}$ ,  $\kappa$  is an additional model parameter in  $\text{veh}/\text{km}/\text{lane}$ ,  $\nu_{\min}$  is the minimum value of the speed in  $\text{km}/\text{hr}$ ,  $\nu_f$  is the free- flow speed in  $\text{km}/\text{hr}$ ,  $\rho_{\text{cr}}$  refers to the critical density in  $\text{veh}/\text{km}$ , and  $q_{\text{cap}}$  means the capacity in  $\text{veh}/\text{hr}$ .

**Table 3.1**  
*Optimal Parameter Values for June 9, 2022 (Normal Weather Condition)*

Model Parameters	Value
$\tau$ (s)	8.121
$\nu$ ( $\text{km}^2/\text{h}$ )	29.000
$\delta$ ( $\text{h}/\text{km}$ )	0.118
$\Phi$ ( $\text{h}/\text{km}$ )	0.00021
$\kappa$ ( $\text{veh}/\text{km}/\text{lane}$ )	2.337
$\nu_{\min}$ ( $\text{km}/\text{hr}$ )	12.159
$\nu_f$ ( $\text{km}/\text{hr}$ )	83.225
$\rho_{\text{cr}}$ ( $\text{veh}/\text{km}$ )	21.402
$q_{\text{cap}}$ ( $\text{veh}/\text{hr}$ )	1781.210

Figure 3.1 shows the congestion tracking performance on June 9 using only 1 Fundamental Diagram. It illustrates the modeling outcomes for traffic flows and mean speeds. It presents the calibration results for flows and speeds at all sensor locations in the study area. In these figures, black refers to actual measurements, while red refers to the modeling results. The calibrated flow models closely predicted the actual data at different locations, while the mean speed models effectively matched when the congestion was formed and when it dissipated. It is evident that flow prediction is more accurate than with mean speeds. This is due to the governing conservation equation for traffic volumes which is unaffected by free flow speeds. On the other hand, average speeds are greatly affected by these.

It highlights the congestion events in the study area. The event started at detector 16 and spread downstream to detector 13 at around 6:45 AM to 8:30 AM. The congestion

428 event was accurately predicted in terms of spatiotemporal coverage. The results are  
429 considered satisfactory to be applied further. Note that the model has been arranged in  
430 downstream-to-upstream form.

431  
432 Figure 3.2 shows the space-time maps depicting the coverage of the dynamics of flows  
433 and average speeds in the highway section, in which the y-axis represents the spacing  
434 requirements in the traffic flow direction. When comparing it to the actual data, the  
435 models under calibration effectively captured traffic flow dynamics and reproduced the  
436 emergence and dissipation of the congestion wave.

437  
438 **3.1.2 Considering Heterogeneity**

440 Considering traffic flow inhomogeneity means that a unique fundamental diagram (FD)  
441 is assigned to a segment of the highway. This highlights how variations in key traffic  
442 flow parameters reflect traffic flow differences across the study area.

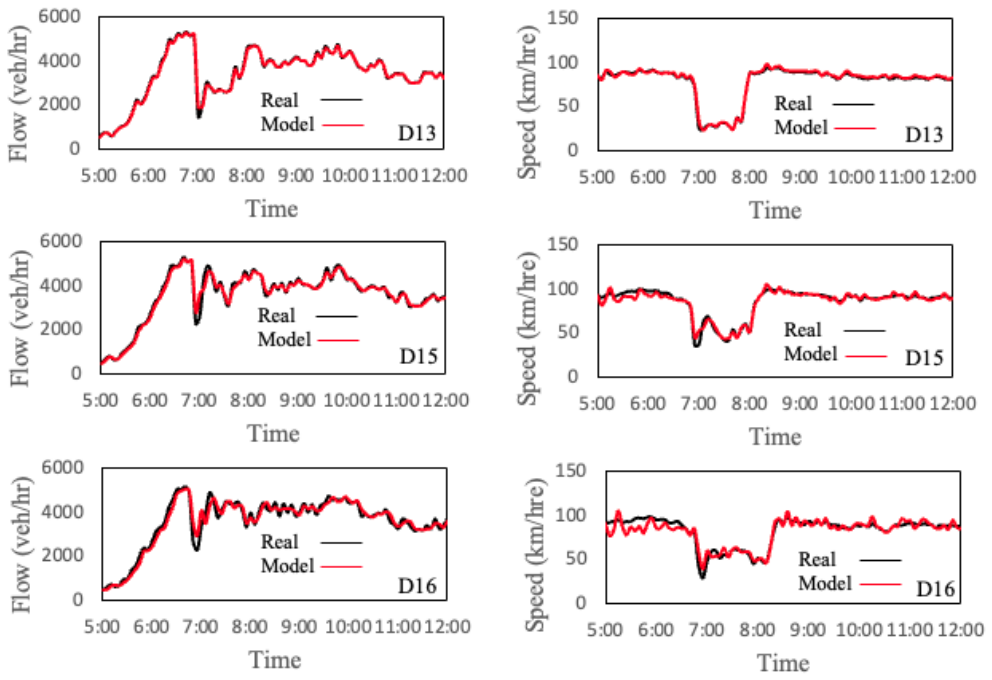
443  
444 Five calibration runs were again conducted and their performance is measured in terms  
445 of MAPE for all the detectors. The same with the consideration of the same fundamental  
446 diagram for each section, the algorithm began with a similar initial value with the  
447 working simplex generated by randomly generating succeeding values around this  
448 initial point. The result shows best performance of all the calibration runs has a MAPE  
449 of 1.3152 %, 2.8912 %, and 5.5827 % for Detectors 13, 15, and 16, respectively. Again,  
450 the difference in the performance index between each run is not very significant which  
451 shows that the algorithm can converge to almost the same optimal values.

452  
453 The modeling result in terms of congestion tracking is shown in Figure 3.3. It illustrates  
454 the modeling outcomes for traffic flows and mean speeds for June 9, 2022 considering  
455 heterogeneity. It presents the calibration results for flows and speeds at all sensor  
456 locations in the study area. In these figures, black refers to actual measurements, while  
457 red refers to the modeling results. The calibrated flow models in closely predicted the  
458 actual data at different locations, while the mean speed models effectively matched  
459 when the congestion was formed and when it dissipated. Flow prediction is more  
460 accurate than with mean speeds due to the conservation equation being the same as the  
461 result of considering only 1 fundamental diagram.

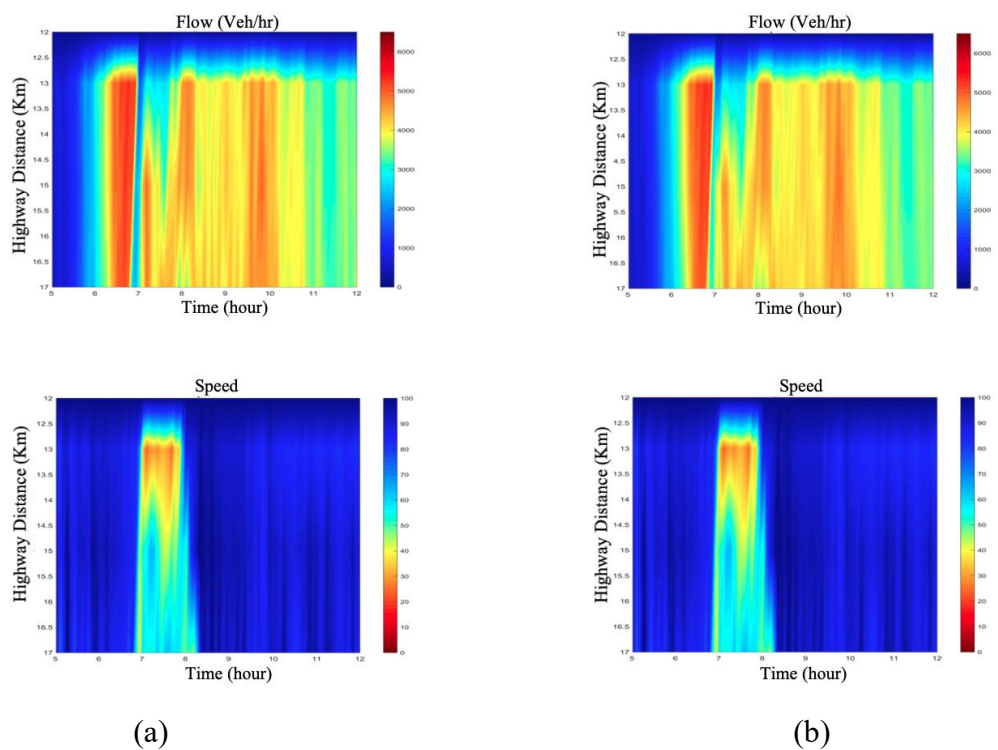
462  
463 Figure 3.4 shows the space-time maps depicting the coverage of the dynamics of flows  
464 and average speeds in the highway section, in which the y-axis represents the spacing  
465 requirements in the traffic flow direction. When comparing it to the actual data, the  
466 models under calibration effectively captured traffic flow dynamics and reproduced  
467 traffic congestion with appropriate strength over the relevant spatiotemporal range. This  
468 highlights the congestion events in the study area. The event started at detector 16 and  
469 spread downstream to the detector 13 at around 6:45 AM to 8:30 AM. The congestion  
470 event was accurately predicted in terms of spatiotemporal coverage.

471  
472  
473  
474  
475 **Figure 3.1 Results of Model Calibration of flows and speeds at Different Sensor**  
476 **Locations – June 9, 1 FD**

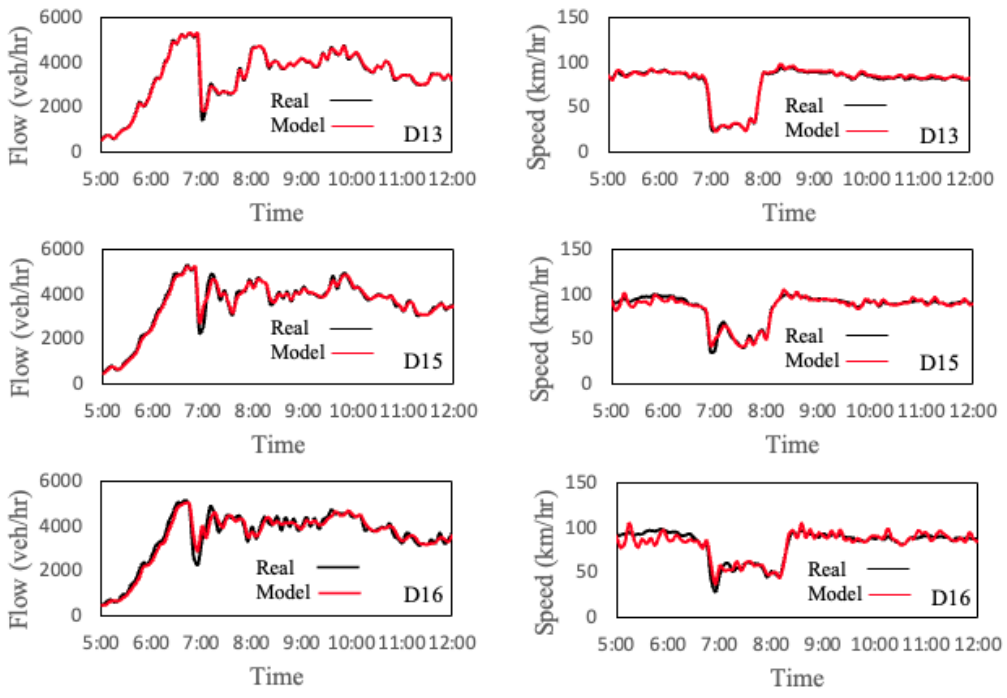
477



478  
479  
480  
481 **Figure 3.2** Space-time evolution of flows and speeds along the study area (a) real  
482 data; (b) using 1 Fundamental Diagram  
483



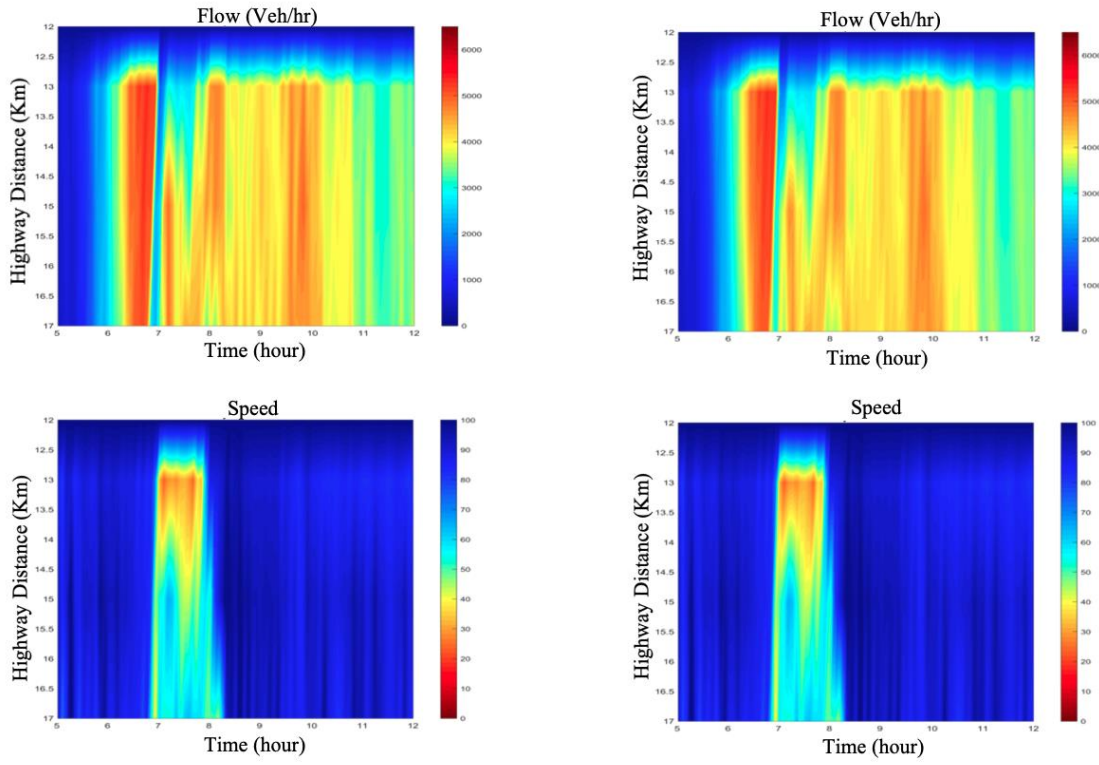
484  
485  
486 **Figure 3.3** Results of Model Calibration Flows and Speeds at Different Sensor  
487 Locations – June 9, 3 FD  
488



489  
490

491  
492  
493

**Figure 3.4** Space-time evolution of flows along the study area (a) actual data; (b) using 3 Fundamental Diagrams



494  
495  
496

(a)

(b)

### 3.29 **I** Summary of results in consideration of traffic flow heterogeneity

498 Table 3.2 summarizes the performance of the best calibration runs in terms of MAPE  
 499 of speed in km/hr for all the detectors in consideration of traffic flow heterogeneity.  
 500 The result shows that considering traffic flow heterogeneity in traffic flow modeling  
 501 has an advantage, as shown in the decrease in the value of MAPE. This result is  
 502 expected because of the increase in the number of degrees of freedom. Nevertheless,  
 503 this difference between the performances is only slight and can be considered not  
 504 significant. This is different compared to the result obtained by (Wang et al., 2022)  
 505 where the consideration of different fundamental diagrams resulted in a significant  
 506 difference in the performance indicators. This can be explained by their use of the  
 507 whole expressway network which consisted of different sections with different  
 508 geometric characteristics. In the current study, the span of the highway considered  
 509 consists of the same number of lanes and other geometric characteristics which  
 510 justifies that they can have the same fundamental diagram. With this, further  
 511 application in the next sections will only consider one fundamental diagram for the  
 512 traffic flow modeling in the considered study area.

513 **Table 3.2**

514  
 515 *Performance summary for 5 calibration runs on June 9, 2022 considering traffic flow  
 516 heterogeneity*

Heterogeneity Consideration	Detector No.	MAPE
1 FD	D13	1.3943
	D15	3.1043
	D16	5.7205
3 FD	D13	1.3152
	D15	2.8912
	D16	5.5827

519  
 520  
 521  
 522  
 523 The space-time diagram for flows and speed using 1 and 3 fundamental diagrams shows  
 524 that both models were able to predict when congestion forms and dissipates in the  
 525 spatiotemporal range and that the speed and flow prediction matches are both  
 526 acceptable for further application. Overall, the congestion tracking results under normal  
 527 weather were very satisfactory.

528

529

### 530 **3.2 Model Calibrations under Rainy Weather Conditions**

531

532 The calibration process was also performed using measurement data on a rainy day on  
 533 Sept 26, 2022. The same 5 runs are completed and the calibration performance in terms  
 534 of MAPE for speed is determined. The same as the calibration for normal weather  
 535 conditions, there is not a significant difference in the MAPE showing that the algorithm  
 536 converges to almost the same parameter values. The result shows that the performance  
 537 of the calibration has a MAPE of 3.1673 %. The resulting parameters of the model are

538 shown in Table 3.4. It should be noted that there is a substantial decrease in the key  
 539 traffic flow parameters of free-flow speed  $v_f$ , critical density  $\rho_{cr}$ , and  $q_{cap}$ . To illustrate,  
 540 the free-flow speed, critical density, and capacity under normal weather conditions are  
 541 83.2 km/hr, 21.4 veh/km, and 1781.2 veh/hr, respectively. Under bad weather  
 542 conditions, it was reduced to 72.3 km/hr, 21 veh/km, and 1510 veh/hr. respectively.  
 543 This is expected since it has been proven in the literature that weather conditions affect  
 544 the key traffic flow parameters and are consistent with empirical observations.

545

546

547 **Table 3.4**

548

549 *Optimal Parameter Values for September 26, 2022 (Bad Weather Conditions)*

550

551

Model Parameters	Value
$\tau$ (s)	6.25
$v$ (km <sup>2</sup> /h)	27.99
$\delta$ (h/km)	0.20
$\Phi$ (h/km)	0.00
$\kappa$ (veh/km/lane)	10.00
$v_{min}$ (km/hr)	10.00
$v_f$ (km/hr)	72.26
$\rho_{cr}$ (veh/km)	21.00
$q_{cap}$ (veh/hr)	1510.71

552

553

554 With the same study area which has homogeneous traffic flow, the modeling results  
 555 exhibited similar calibration accuracy for flows on a rainy day compared to a non-rainy  
 556 day. The model was still able to match the real flow and speed data including the  
 557 tracking when congestion emerged and dissipated. However, the accuracy of speed  
 558 calibration on rainy days was somewhat reduced.. The modeling results for flows and  
 559 mean speeds are shown in Figure 3.5 while the space-time diagram for flows and speeds  
 560 is illustrated in Figure 3.6.

561

562

563 **3.3 Validation of METANET under Different Weather Conditions**

564

565 Both the validation results for flows and speeds under different weather conditions are  
 566 shown in this section. In each pair of the following validation processes, the optimal  
 567 model parameters for each weather condition are used for a given date. It is first  
 568 validated using calibration results from the same weather condition and another  
 569 validation process is conducted using the calibration results from a different weather  
 570 condition. Note that the accompanying parameters for a given weather condition are  
 571 used (see Tables 3.1 and 3.3).

572

573 For each type of weather, 3 days were used for validation purposes. For normal weather  
 574 conditions, June 17, 2022; June 20, 2022; and June 29, 2022 were used. For bad weather  
 575 conditions, June 30, 2022; October 6, 2022; and October 7, 2022, were validated. For

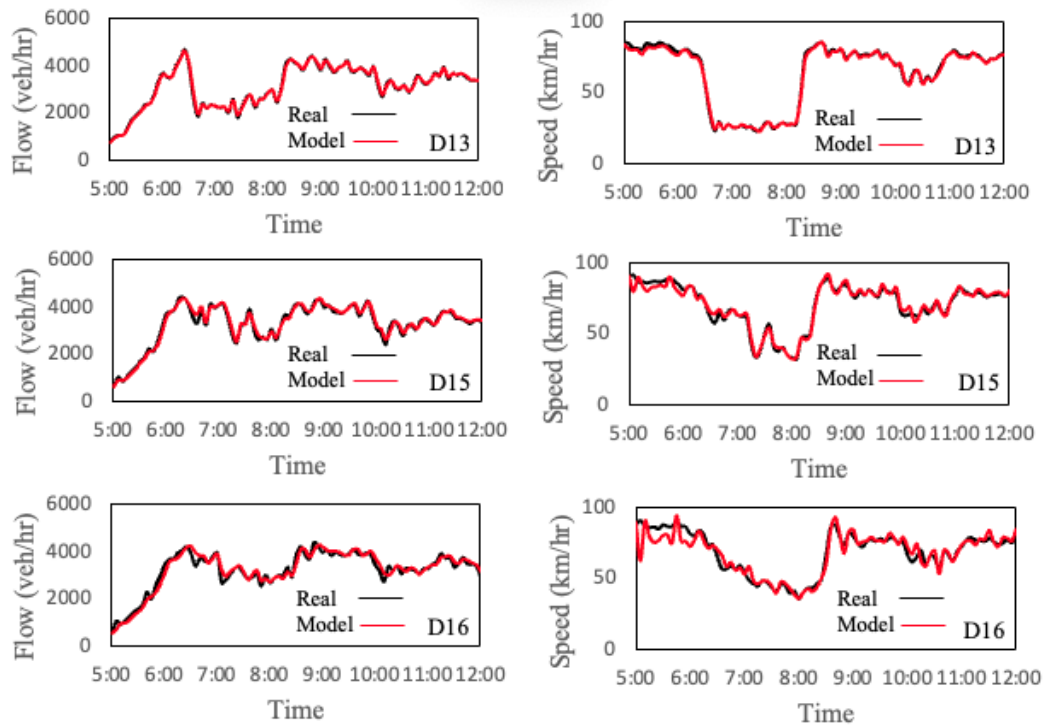
576 a given day, the modeling spanned from the same time interval during the calibration  
577 process.

578

579

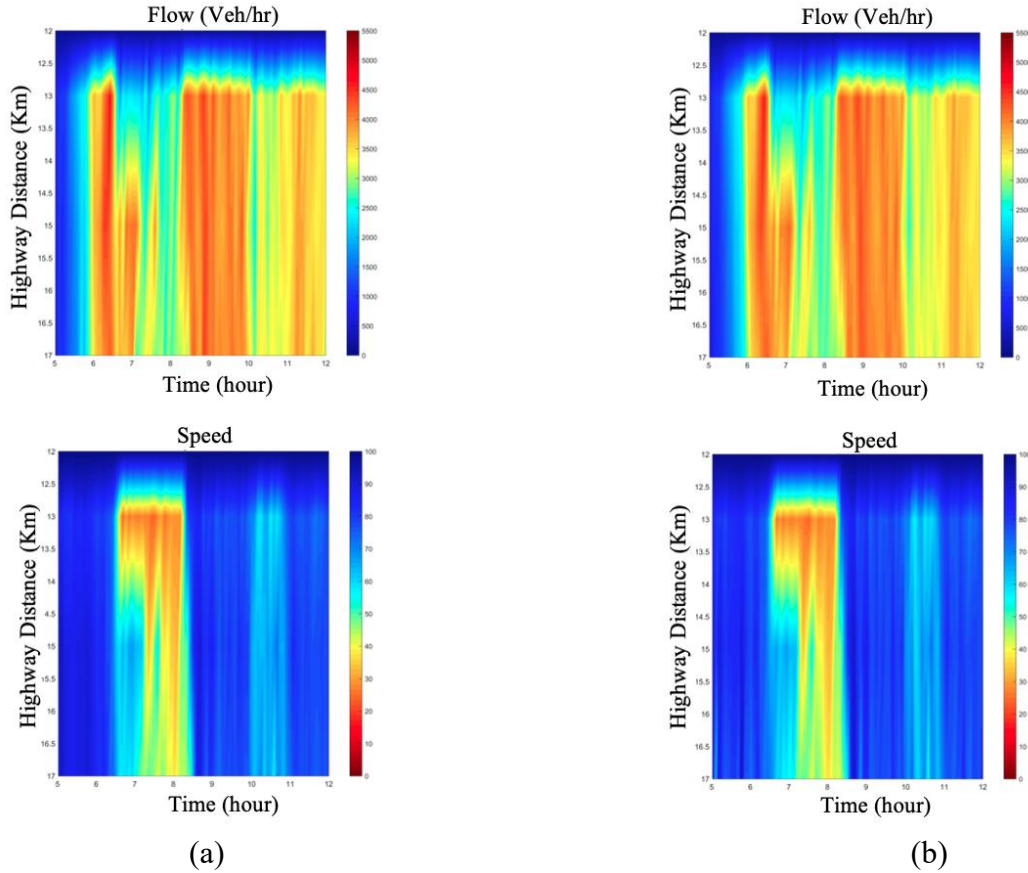
580 **Figure 3.5 Results of Model Calibration (Flows and Speeds) at Different Sensor  
581 Locations – Sept 26**

582



583

584 **Figure 3.6** Space-time evolution of flows along the study area on Sept 26 (a) real  
585 data; (b) model



586  
587

(a)

(b)

588  
589  
590

### 3.3.1 Validation on days with no rain

591 The validation of the model under normal weather conditions for 3 days on June 17,  
592 2022; June 20, 2022; and June 29, 2022, is discussed in this section. Table 3.4 shows  
593 the detailed quantitative error measurement in terms of MAPE for comparison.  
594 Weather-specific means that the model parameters used in the validation are the  
595 calibration results under normal weather conditions (see Table 3.1). On the other hand,  
596 non-weather-specific means that the validation model parameters used are those  
597 derived under the calibration of a day with bad weather conditions (see Table 3.4). It is  
598 shown that weather-specific validation always performs better than the non-weather-  
599 specific modeling results. To illustrate, the MAPE for June 17 using calibration results  
600 from June 9 with the same weather conditions is 5.0615% while the MAPE for June 17  
601 using calibration results from September 26 which has a different weather condition  
602 drastically increased to 14.0573 %. This result also proves that the modeling result is  
603 sensitive to the value of the key traffic flow parameters since it was found in the  
604 previous section that there is a significant decrease in the value of the said parameters  
605 under different weather conditions. It is worth noting that the validation results under  
606 the same weather conditions have less accuracy compared to the calibration.  
607 Nevertheless, the difference between weather-specific validation processes is very  
608 significant. It can be concluded that considering the weather in the validation process  
609 of METANET will be more helpful for further practical applications.

610

611 For brevity, only the modeling results on June 17 are shown but the modeling  
 612 performance for the rest of the days are already shown in Table 3.4. In terms of  
 613 congestion tracking, weather-specific models were able to sufficiently track the  
 614 occurrence and dissipation of the congestion as illustrated in Figure 3.7. This is not the  
 615 case for non-weather-specific modeling depicted in Figure 3.8 which shows that the  
 616 model was not able to replicate the congestion wave at around 6:30 AM. Figure 3.9  
 617 further illustrates the better performance of the weather-specific modeling as shown in  
 618 the space-time heat maps for both flows and speeds sufficiently predicting the  
 619 spatiotemporal values compared to non-weather-specific results.

620

621 *Table 3.4 Summary of results of METANET validation under normal weather  
 622 conditions in terms of MAPE (%)*

Date	Weather-Specific	Non-Weather-Specific
June 17, 2022	5.0615	14.0573
June 20, 2022	12.4080	15.2733
June 29, 2022	10.8848	11.8386

623

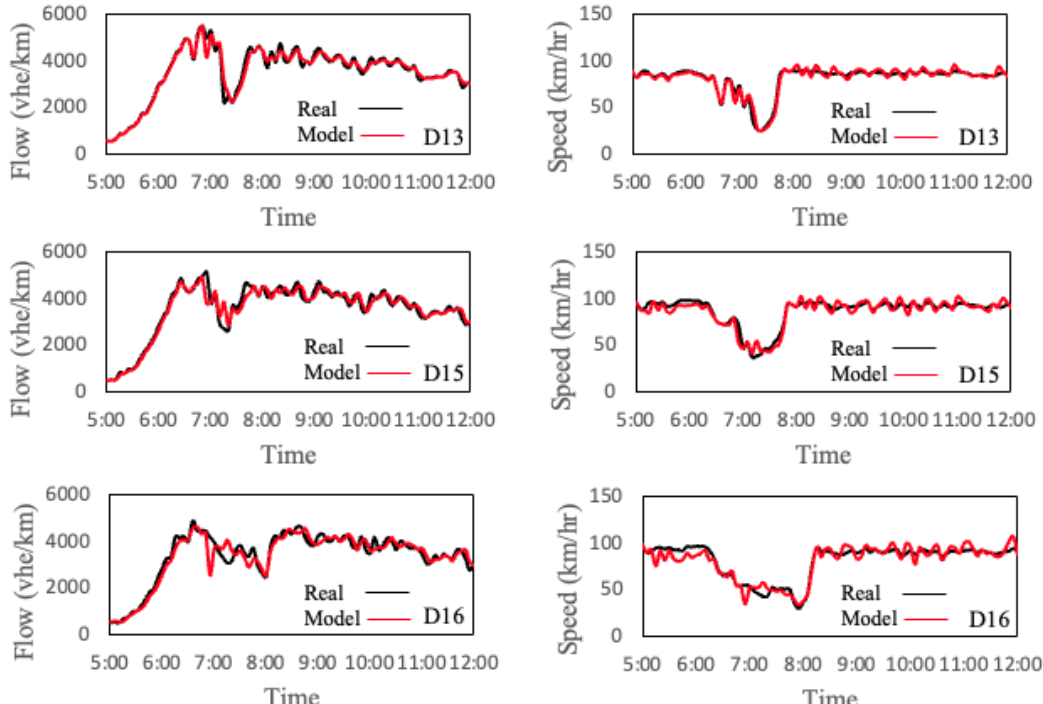
624

625

### 626 **Figure 3.7**

627

628 *Weather-specific validation of flows on June 17, 2022.*

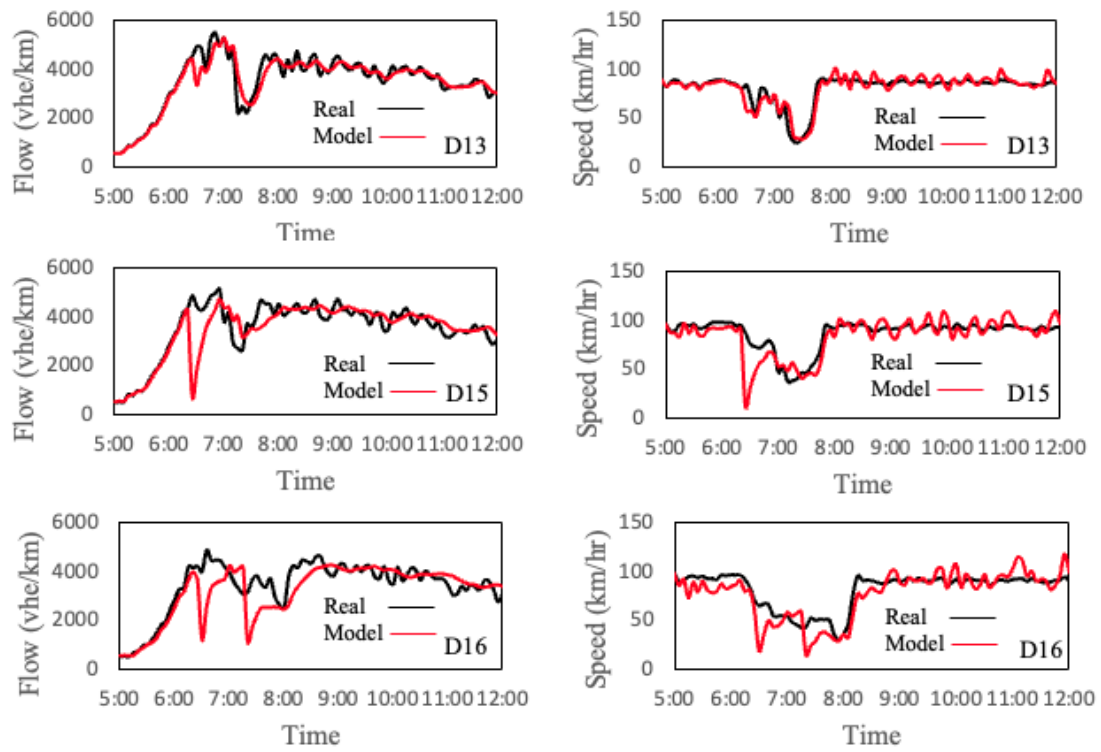


629

630 **Figure 3.8**

631

632 *Non- Weather specific validation offlows on June 17, 2022.*



633

634

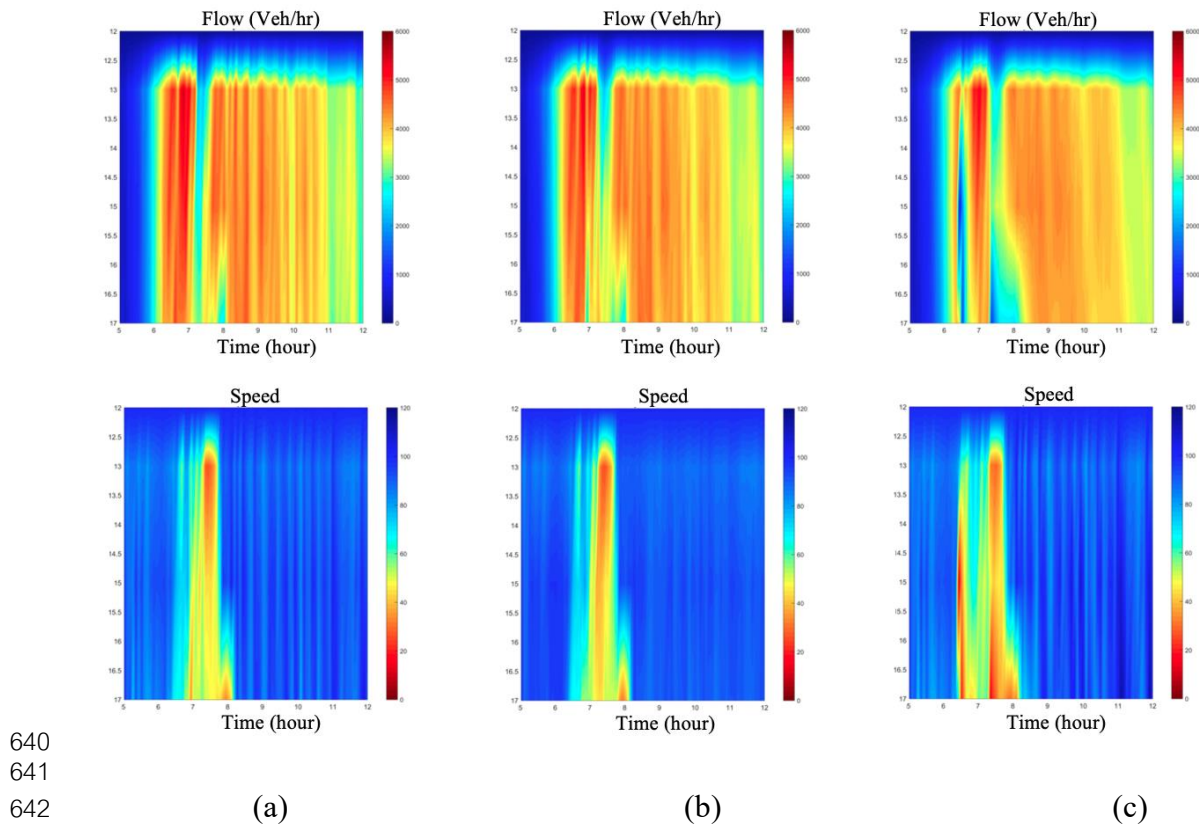
**Figure 3.9**

635

636 *Spatiotemporal evolution of flows on June 17, 2022 along the study area (a) real*  
637 *data; (b) weather-specific validation (c) non-weather-specific validation*

638

639



640  
641  
642

(a)

(b)

(c)

643  
644  
645

### 3.3.2 Validation of data under bad weather conditions.

646 Data from June 30, October 6, and October 6 which experienced bad weather  
647 conditions, were also validated using the calibration results from September 6 with the  
648 same rainy weather conditions. Then, the same data were validated using calibration  
649 results from June 9 with normal weather conditions. The performance summary of the  
650 validation process is summarized in Table 3.5. Weather-specific means that the model  
651 parameters used in the validation are the calibration result under rainy weather  
652 conditions on September 26, 2022. On the other hand, non-weather-specific means that  
653 the validation model parameters used are those derived under the calibration of a day  
654 with normal weather conditions on June 9, 2022. The results show that weather-specific  
655 validation always performs better than the non-weather-specific modeling results. This  
656 illustrates that weather-specific modeling performs more satisfactorily than non-  
657 weather-specific considerations. As an example, the MAPE for June 30 using  
658 calibration results from June 9 with the same weather conditions is 3.13% while the  
659 MAPE for June 30 using calibration results from September 26 which has a different  
660 weather condition drastically increased to 14.27 %.

661

662 For brevity, only the modeling results on June 30 are shown but the modeling  
663 performance for the rest of the days are already shown in Table 3.5. In terms of  
664 congestion tracking, weather-specific models were also able to sufficiently track the  
665 occurrence and dissipation of the congestion as illustrated in Figure 3.10 which is not  
666 the case for non-weather-specific modeling shown in Figure 3.11 which was not able  
667 to reflect the start of the congestion wave. Figures 3.12 further shows the better  
668 performance of the weather-specific modeling as shown in the space-time heat maps

669 for both flows and speeds sufficiently predicting the spatiotemporal values compared  
670 to non-weather-specific results.

671

672

673 **Table 3.5 Summary of results of METANET validation under bad weather conditions**  
674 *in terms of MAPE (%)*

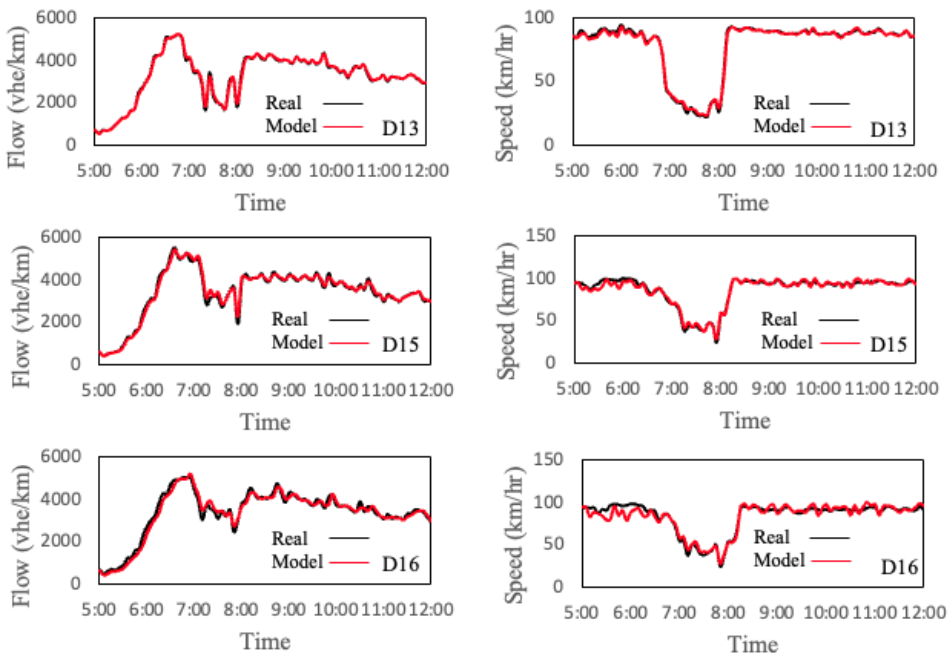
Date	Weather-Specific	Non-Weather-Specific
<b>June 30, 2022</b>	3.13	14.27
<b>October 6, 2022</b>	8.52	11.88
<b>October 7, 2022</b>	7.79	13.05

675

676 **Figure 3.10**

677 *Weather-specific validation of flows on June 30, 2022*

678



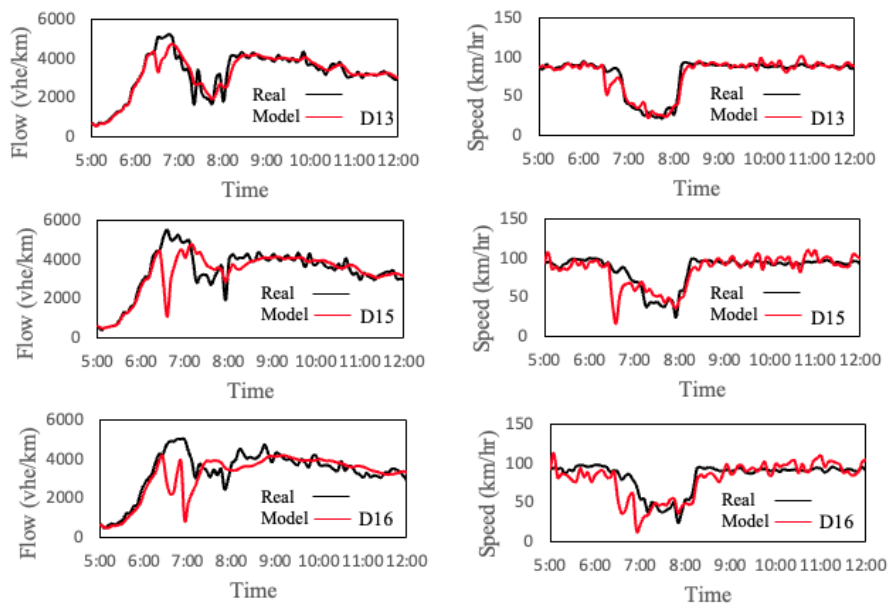
679

680

681

**Figure 3.11**

682

*Non- Weather specific validation of flows on June 30, 2022*

683

684

685

686

687

**Figure 3.12**

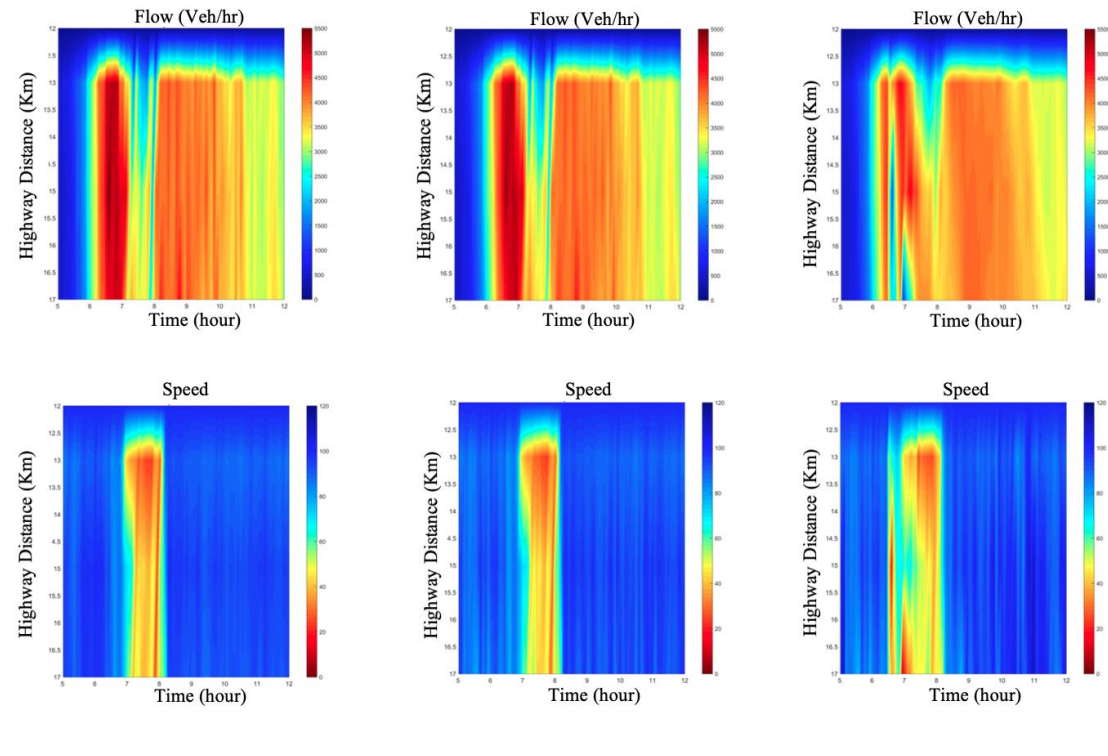
688

*Spatiotemporal evolution of flows on June 30, 2022 along the study area (a) real*

689

*data; (b) weather-specific validation (c) non-weather-specific validation*

690



691

692

693

694

695

(b)

(b)

(c)

696 **4. CONCLUSIONS AND FUTURE WORK**

697  
698 The study confirmed that the METANET model can accurately simulate traffic  
699 dynamics under normal and adverse weather conditions, providing robust calibration  
700 and validation results. This capability makes METANET a reliable tool for forecasting  
701 traffic behavior in real-world environments, particularly in regions with frequent  
702 rainfall. The research further identifies critical parameters such as free-flow speed,  
703 capacity, and critical density that significantly influence the model's performance.  
704 Adjustments to these parameters enhance METANET's ability to adapt to weather-  
705 induced changes in traffic flow, providing a practical foundation for developing more  
706 accurate, weather-responsive traffic management systems.

707 Moreover, METANET demonstrated strong potential in tracking congestion even under  
708 varying rainfall intensities. The model effectively captured key weather-induced  
709 changes, such as reduced free-flow speed and capacity. These findings validate  
710 METANET's adaptability to complex traffic phenomena and show its potential in  
711 supporting proactive, data-driven traffic management.

712  
713 We have replicated the performance of the METANET model in the prediction of traffic  
714 states both for calibration and validation as shown in previous studies. To our  
715 knowledge, this is the first time that the model was used using data from Bangkok,  
716 Thailand. This shows that METANET-based control and operations strategies can  
717 apply to the area.

718  
719 The study indicated that accounting for traffic flow heterogeneity impacts model  
720 performance. However, the improvement observed was minimal, likely due to the study  
721 focusing on a limited segment of the expressway network and the relatively  
722 homogeneous nature of the study area. Future research should incorporate traffic flow  
723 heterogeneity or use multiple fundamental diagrams in traffic dynamics modeling. It is  
724 anticipated that performance enhancements will be more significant when applied to  
725 larger study areas.

726  
727 The model successfully replicated and tracked congestion patterns under both normal  
728 and adverse weather conditions. However, it revealed a notable decrease in key traffic  
729 flow parameters, especially free-flow speed and capacity during rainy conditions.

730  
731 Our findings also highlight the model's sensitivity to key traffic flow parameters, which  
732 were observed to change considerably under different weather conditions. Although  
733 validation results under the same weather conditions are less accurate compared to  
734 calibration performance, the difference in performance between weather-specific and  
735 non-weather-specific models is substantial. Therefore, incorporating weather  
736 considerations into METANET's validation process enhances its practical  
737 applicability.

738  
739 In terms of model validation, weather-specific modeling consistently outperformed the  
740 validation without considering weather factors. Weather-specific models effectively  
741 captured both the onset and dissipation of congestion and accurately predicted  
742 spatiotemporal values. In contrast, non-weather-specific models failed to replicate the  
743 congestion waves.

746 This study advances the understanding of how weather conditions, particularly rainfall,  
747 affect traffic flow parameters and dynamics. By enhancing predictive models for traffic  
748 management and control strategies, the research contributes to the development of  
749 resilient systems that maintain efficiency and safety during adverse weather. Notably,  
750 it is the first comprehensive study to incorporate extensive rainfall data, offering a  
751 robust and longitudinal perspective on rainy conditions. This approach addresses gaps  
752 in previous research, which either assumed clear weather or analyzed limited rainy-day  
753 data, yielding incomplete conclusions.

754  
755 A significant focus of the study is the rigorous evaluation of the METANET model  
756 under varying weather conditions. By assessing its calibration and validation accuracy,  
757 sensitivity to parameter variations, and ability to replicate traffic flow characteristics  
758 such as congestion tracking, the research highlights the model's adaptability. The  
759 innovative use of multiple fundamental diagrams in the calibration process further  
760 improves the model's robustness across different traffic regimes and weather scenarios.  
761 Additionally, the study includes a practical sensitivity analysis, identifying parameters  
762 most affected by adverse weather, enabling traffic engineers to refine models, optimize  
763 signal control, enhance route guidance, and develop adaptive traffic management  
764 strategies.

765  
766 The findings have significant practical applications in traffic management and urban  
767 planning. They provide insights into designing resilient infrastructure, such as weather-  
768 protected lanes, improved drainage systems, and real-time road monitoring  
769 technologies. Real-time traffic control systems informed by this research can  
770 dynamically adjust speed limits, issue warnings through variable message signs, and  
771 respond to rainfall, reducing accidents and managing congestion effectively.  
772 Furthermore, the refined METANET parameters improve the predictive accuracy of  
773 traffic patterns, aiding resource allocation during adverse weather conditions.

774  
775 Overall, this study offers a deeper understanding of how weather influences traffic  
776 congestion. The findings support the development of weather-responsive strategies that  
777 enhance road safety, efficiency, and resilience, ultimately benefiting traffic  
778 management, urban planning, and real-time control systems in mitigating the impacts  
779 of inclement weather.

780  
781 The METANET model, while effective for macroscopic traffic flow modeling, has  
782 limitations in capturing intricate vehicle interactions in high-density or complex  
783 scenarios, such as urban congestion or merging behaviors. Calibration for this study  
784 used data from the Burapha Whiti Expressway in Bangkok, making the parameters  
785 specific to that roadway and less generalizable to other networks with different  
786 geometries, lane configurations, or environmental conditions. The reliance on the  
787 Nelder-Mead optimization method may have further limited the findings due to  
788 convergence on local minima.

789  
790 The study analyzed clear and rainy weather but excluded other factors like temperature,  
791 wind, or seasonal variations, which could also affect traffic. Low-resolution microwave  
792 radar data collected every five minutes may have missed short-term fluctuations,  
793 reducing the model's sensitivity to finer changes in traffic flow. Future research could  
794 address these gaps by incorporating higher-resolution or additional data sources and  
795 exploring a broader range of environmental conditions.

796 Future studies could also explore integrating METANET with adaptive and predictive  
797 control strategies, such as ramp metering, variable speed limits, and coordinated signal  
798 timings. These enhancements would improve real-time congestion management and  
799 expand the model's applicability to diverse and complex traffic scenarios.

800

801

802

## 803 5. REFERENCES

804 Bie, Y., Qiu, T. Z., Zhang, C., & Zhang, C. (2017). Introducing Weather Factor Modelling into Macro  
805 Traffic State Prediction. *Journal of Advanced Transportation*, 2017, 1–15.  
806 <https://doi.org/10.1155/2017/4879170>

807 Courant, R., Friedrichs, K., & Lewy, H. (1928). Über die partiellen Differenzengleichungen der  
808 mathematischen Physik. *Mathematische Annalen*, 100(1), 32–74.  
809 <https://doi.org/10.1007/BF01448839>

810 Daganzo, C. F. (1994). The cell transmission model: A dynamic representation of highway traffic  
811 consistent with the hydrodynamic theory. *Transportation Research Part B: Methodological*,  
812 28(4), 269–287. [https://doi.org/10.1016/0191-2615\(94\)90002-7](https://doi.org/10.1016/0191-2615(94)90002-7)

813 de Moura, C. A., & Kubrusly, C. S. (Eds.). (2013). *The Courant–Friedrichs–Lewy (CFL) Condition*.  
814 Birkhäuser Boston. <https://doi.org/10.1007/978-0-8176-8394-8>

815 Kan, Y., Wang, Y., Papageorgiou, M., & Papamichail, I. (2016). Local ramp metering with distant  
816 downstream bottlenecks: A comparative study. *Transportation Research Part C: Emerging  
817 Technologies*, 62, 149–170. <https://doi.org/10.1016/j.trc.2015.08.016>

818 Kontorinaki, M., Spiliopoulou, A., Roncoli, C., & Papageorgiou, M. (2017). First-order traffic flow  
819 models incorporating capacity drop: Overview and real-data validation. *Transportation Research  
820 Part B: Methodological*, 106, 52–75. <https://doi.org/10.1016/j.trb.2017.10.014>

821 Kotsialos, A., Papageorgiou, M., Diakaki, C., Pavlis, Y., & Middleham, F. (2002). Traffic flow  
822 modeling of large-scale motorway networks using the macroscopic modeling tool METANET.  
823 *IEEE Transactions on Intelligent Transportation Systems*, 3(4), 282–292.  
824 <https://doi.org/10.1109/TITS.2002.806804>

825 Lagarias, J. C., Reeds, J. A., Wright, M. H., & Wright, P. E. (1998). Convergence Properties of the  
826 Nelder–Mead Simplex Method in Low Dimensions. *SIAM Journal on Optimization*, 9(1), 112–  
827 147. <https://doi.org/10.1137/S1052623496303470>

828 Lighthill, M., & Whitman, G. (1955). On kinematic waves II. A theory of traffic flow on long crowded  
829 roads. *Proceedings of the Royal Society of London. Series A. Mathematical Physical Sciences*,  
830 317–345.

831 Messmer, A., & Papageorgiou, M. (1990). METANET: A macroscopic simulation program for  
832 motorway networks. *Traffic Engineering and Control*, 31(9).

833 Mohammadian, S., Zheng, Z., Haque, Md. M., & Bhaskar, A. (2021). Performance of continuum  
834 models for realworld traffic flows: Comprehensive benchmarking. *Transportation Research Part  
835 B: Methodological*, 147, 132–167. <https://doi.org/10.1016/j.trb.2021.03.007>

836 Nelder, J. A., & Mead, R. (1965). A Simplex Method for Function Minimization. *The Computer  
837 Journal*, 7(4), 308–313. <https://doi.org/10.1093/comjnl/7.4.308>

838 Ngoduy, D., & Maher, M. J. (2012). Calibration of second order traffic models using continuous cross  
839 entropy method. *Transportation Research Part C: Emerging Technologies*, 24, 102–121.  
840 <https://doi.org/10.1016/j.trc.2012.02.007>

841 Papageorgiou, M., Blosseville, J.-M., & Hadj-Salem, H. (1989). Macroscopic modelling of traffic flow  
842 on the Boulevard Périphérique in Paris. *Transportation Research Part B: Methodological*, 23(1),  
843 29–47. [https://doi.org/10.1016/0191-2615\(89\)90021-0](https://doi.org/10.1016/0191-2615(89)90021-0)

844 Papageorgiou, M., Papamichail, I., Messmer, A., & Wang, Y. (2010). *Traffic Simulation with  
845 METANET* (pp. 399–430). [https://doi.org/10.1007/978-1-4419-6142-6\\_11](https://doi.org/10.1007/978-1-4419-6142-6_11)

846 Payne, H. (1971). Models of Freeway Traffic and Control. *Mathematical Models of Public Systems*, 1,  
847 51–61.

848 Richards, P. (1956). Shock Waves on the Highway. *Operations Research*, 4, 42–51.

849 Rubinstein, R., & Kroese, D. (2004). *The cross-entropy method: a unified approach to combinatorial  
850 optimization, Monte-Carlo simulation, and machine learning* (Vol. 133). Springer.

851 Sanz-Serna, J. M., & Spijker, M. N. (1986). Regions of stability, equivalence theorems and the  
852 Courant-Friedrichs-Lowy condition. *Numerische Mathematik*, 49(2–3), 319–329.  
853 <https://doi.org/10.1007/BF01389633>

854 Spiliopoulou A., Papamichail I., Papageorgiou M. and Chrysoulakis, J., “CALISTO user’s manual”,  
855 Deliverable 4.1, Technical Report for the Project SMOOTH, ARCHIMEDES III, Athens, July  
856 2014.

857 Spiliopoulou, A., Kontorinaki, M., Papageorgiou, M., & Kopelias, P. (2014). Macroscopic traffic flow  
858 model validation at congested freeway off-ramp areas. *Transportation Research Part C:*  
859 *Emerging Technologies*, 41, 18–29. <https://doi.org/10.1016/j.trc.2014.01.009>

860 Spiliopoulou, A., Papamichail, I., Papageorgiou, M., Tyrinopoulos, Y., & Chrysoulakis, J. (2017).  
861 Macroscopic traffic flow model calibration using different optimization algorithms. *Operational*  
862 *Research*, 17(1), 145–164. <https://doi.org/10.1007/s12351-015-0219-4>

863 Wang, Y., Kosmatopoulos, E. B., Papageorgiou, M., & Papamichail, I. (2014). Local Ramp Metering  
864 in the Presence of a Distant Downstream Bottleneck: Theoretical Analysis and Simulation Study.  
865 *IEEE Transactions on Intelligent Transportation Systems*, 15(5), 2024–2039.  
866 <https://doi.org/10.1109/TITS.2014.2307884>

867 Wang, Y., Yu, X., Guo, J., Papamichail, I., Papageorgiou, M., Zhang, L., Hu, S., Li, Y., & Sun, J.  
868 (2022). Macroscopic traffic flow modelling of large-scale freeway networks with field data  
869 verification: State-of-the-art review, benchmarking framework, and case studies using  
870 METANET. *Transportation Research Part C: Emerging Technologies*, 145, 103904.  
871 <https://doi.org/10.1016/j.trc.2022.103904>

872 Wang, Y., Yu, X., Zhang, S., Zheng, P., Guo, J., Zhang, L., Hu, S., Cheng, S., & Wei, H. (2021).  
873 Freeway Traffic Control in Presence of Capacity Drop. *IEEE Transactions on Intelligent*  
874 *Transportation Systems*, 22(3), 1497–1516. <https://doi.org/10.1109/TITS.2020.2971663>

875 Whitley, D. (1994). A genetic algorithm tutorial. *Statistics and Computing*, 4(2).  
876 <https://doi.org/10.1007/BF00175354>

877 Whitman, G. B. (1974). *Linear and Non-linear Waves*. Wiley.

878 Zhao, M. (2021). *Development of Hypersonic Aerothermodynamic Technologies* (pp. 1–23).  
879 [https://doi.org/10.1007/978-981-33-6526-1\\_1](https://doi.org/10.1007/978-981-33-6526-1_1)

880